Blood Flow Magnetic Resonance Imaging of Retinal Degeneration

Yingxia Li,[1] *Haiying Cheng,*[1] *Qiang Shen,*[1,2,3,4,5,6] *Moon Kim,*[7] *Peter M. Thule,*[7,8] *Darin E. Olson,*[7,8] *Machelle T. Pardue,*[7,9] *and Timothy Q. Duong*[1,2,3,4,5,6,7]

PURPOSE. This study aims to investigate quantitative basal blood flow as well as hypercapnia- and hyperoxia-induced blood flow changes in the retinas of the Royal College of Surgeons (RCS) rats with spontaneous retinal degeneration, and to compare with those of normal rat retinas.

METHODS. Experiments were performed on male RCS rats at post-natal days P90 ($n = 4$) and P220 ($n = 5$), and on age-matched controls at P90 ($n = 7$) and P220 ($n = 6$). Hyperoxic (100% O_2) and hypercapnic (5% CO_2, 21% O_2, balance N_2) challenges were used to modulate blood flow. Quantitative baseline blood flow, and hypercapnia- and hyperoxia-induced blood flow changes in the retinas were imaged using continuous arterial spin labeling MRI at $90 \times 90 \times 1500$ μm.

RESULTS. In the normal rat retinas, basal blood flow of the whole-retina was 5.5 mL/gram per min, significantly higher than those reported in the brain (~ 1 mL/gram per min). Hyperoxia decreased blood flow due to vasoconstriction and hypercapnia increased blood flow due to vasodilation in the normal retinas. In the RCS rat retinas, basal blood flow was diminished significantly ($P < 0.05$). Interestingly, absolute hyperoxia- and hypercapnia-induced blood flow changes in the RCS retinas were not statistically different from those in the normal retinas ($P > 0.05$). However, blood flow percent changes in RCS retinas were significantly larger than in normal retinas due to lower basal blood flow in the RCS retinas.

CONCLUSIONS. Retinal degeneration markedly reduces basal blood flow but does not appear to impair vascular reactivity. These data also suggest caution when interpreting relative stimulus-evoked functional MRI changes in diseased states where basal parameters are significantly perturbed. Quantitative blood flow MRI may serve as a valuable tool to study the retina without depth limitation. (*Invest Ophthalmol Vis Sci.* 2009;50:1824–1830) DOI:10.1167/iovs.08-2188

Retinitis pigmentosa (RP) is a family of retinal diseases associated with progressive photoreceptor degeneration; it affects ~ 1.5 million people worldwide.[1] The Royal College of Surgeons (RCS) rat[2,3] is an established model of RP due to a mutation in the *Mertk* gene[3] that results in impaired phagocytosis of photoreceptor segments by the retinal pigment epithelium. While RCS rat retinas have been well characterized genetically[3] and histologically,[4–7] the lack of noninvasive imaging techniques has limited the investigation of basal blood flow, oxygenation, functional hemodynamic responses, and temporal progression of this disease in vivo. There is evidence that environmental factors may play an important role in RP progression. Moreover, a number of potential preclinical treatments, including vitamin A supplementation, intravitreal administration of growth factors and neuroprotective drugs,[8] gene therapy,[9] and prosthetics,[10] show evidence of slowing or reversing retinal degeneration. Noninvasive imaging technologies able to image physiological and functional changes of the retina in vivo could improve longitudinal staging, pathophysiologic characterization, and evaluation of therapeutic intervention for retinal degeneration and other retinal diseases.

The retina has most often been studied using optically based imaging techniques. These techniques include fundus and optical coherent tomography[11,12] for imaging anatomy; phosphorescent imaging[13] and intrinsic optical imaging for imaging oxygenation[14–16]; fluorescein angiography,[17] indocyanine green angiography,[18] scanning laser ophthalmoscopy,[19] laser Doppler flowmetry (LDF), and laser speckle imaging[20,21] for imaging blood flow (BF). Optically based imaging techniques require an unobstructed light pathway, and the constrained illumination angle limits the field of view. With the exception of structural assessment by optical coherence tomography,[12] optically based techniques are limited to imaging the retinal surface. Moreover, the above mentioned BF techniques can only measure BF in large or superficial vessels, which may not accurately reflect local tissue perfusion. Choroid BF in the foveal region where retinal vessels are absent has been reported using Heidelberg retina flowmeter,[22] indocyanine green angiography,[23] and the scanning laser ophthalmoscope.[19] Scanning laser ophthalmoscopy has also been used to image flow velocity in different vessels sizes associated with hypoxia and hyperoxia.[24]

In contrast, magnetic resonance imaging (MRI) has a large field of view, no depth limitation and, importantly, can provide structural, physiological (BF and oxygenation), and functional information in a single setting. The drawbacks of MRI are lower spatial resolution and longer acquisition times compared to optically based imaging techniques. Nonetheless, it has recently been demonstrated that MRI can resolve layer-specific retinal anatomy[25–27] and blood oxygenation level-dependent (BOLD) functional MRI responses associated with hypercapnic,[26] hyperoxic,[26] and visual[28] stimulations in the retina. These studies demonstrate that high-resolution MRI of the retina is feasible.

BF by MRI can be made using an exogenous intravascular contrast agent or by magnetically labeling the endogenous water in blood.[29] The latter—commonly referred to as arterial spin labeling (ASL) MRI—yields quantitative BF and dynamic BF changes associated with functional stimulation in normal and diseased brains.[29-31] BF in mL per gram of tissue per minute can be measured on a pixel-by-pixel basis by determining the arterial input function or labeling efficiency without the need for visualizing flow in individual blood vessels. BF MRI to study quantitative basal BF, stimulus-evoked, and pathology-induced BF changes in the brain has been well described.[31-34] However, the small transverse dimension of the retina (267 μm thick, including the choroid[26]), demands very high spatial resolution if such measurements are to be recapitulated in the retina.

It has been well documented in many neurodegenerative diseases that BF in the brain is diminished and its responses to stimulations are compromised.[35-37] These MRI parameters have often served as surrogate markers for disease progression in vivo. We made similar predictions that BF and its responses to stimulation in retinal degeneration are perturbed in the RCS retinas. We used BF MRI to investigate basal BF, and vascular reactivity to oxygen and carbon-dioxide breathing in RCS rat retinas and compared measurements to normal age-matched controls. BF MRI used the continuous ASL technique[31,38] with a separate neck coil for arterial spin labeling and snap-shot echo planar imaging acquisition at 90 $\times$ 90 $\times$ 1500 μm. Quantitative BF measurements allow BF comparison of the retina between experimental groups. BF MRI offers some unique advantages and has the potential to complement existing optical retinal imaging techniques.

MATERIALS AND METHODS

Animal Preparation. All experiments adhered to the ARVO Statement for the Use of Animals in Ophthalmic and Vision Research. Long-Evans RCS rats at post-natal day P90 ($n = 4$) and P220 ($n = 5$) and control normal Long-Evans rats at P90 ($n = 7$) and P220 ($n = 6$) were studied. Complete photoreceptor degeneration is expected by P90 in RCS rats.[5,39] Rats were anesthetized with 1.1% isoflurane, paralyzed with pancuronium bromide (3 mg/kg first dose, 1 mg/kg/hr, ip) and mechanically ventilated. Continuous monitoring of end-tidal CO_2 by capnometer (Surgivet, Waukesha, WI), heart rate and arterial oxygen saturation by pulse oximeter (Nonin-8600; Nonin, Plymouth, MN), and rectal temperature by animal temperature probe (Digisense; Cole Palmer, Vernon Hills, IL) were performed and maintained within normal physiological ranges unless otherwise perturbed. We previously confirmed that air ventilation during baseline measurements maintains normal arterial pO_2.[33,40]

Inhalation Stimuli. Hyperoxic (100% O_2) and hypercapnic (5% CO_2, 21% O_2, balance N_2) challenges were used to modulate BF. Images were acquired continuously for 12 minutes, wherein 6 minutes of data were acquired during baseline (air) and 6 minutes during hyperoxic or hypercapnic challenge. A break of 10 to 15 minutes was given between each stimulus. This duration has been shown previously to be more than sufficient for the systemic circulation to return to baseline as demonstrated by MRI monitoring of BF and oxygenation (i.e., BOLD functional MRI of the brain), exhaled O_2 and CO_2 monitoring, as well as blood-gas measurements in rat studies.[33,41] In the present study, invasive blood-gas sampling was avoided and only end-tidal CO_2, which has been calibrated against blood gases, was monitored and maintained within normal physiological ranges. Typically, two to three trials of hyperoxia and hypercapnia were studied on the same animal and the presentation order was randomized, with the entire study lasting 3 to 4 hours. Basal BF was taken from the baseline measurements before each hypercapnic and hyperoxic challenge.

MRI Methods. MRI studies were performed (Bruker 7-Tesla/30-cm magnet and a 40 G/cm B-GA12 gradient insert, 150 μs risetime;

Bruker, Billerica, MA). Rats were placed onto a head holder consisting of ear and tooth bars. A small circular surface coil (inner diameter ~7 mm) was placed on the left eye. A butterfly neck coil, built into the cradle, was placed at the neck position for continuous arterial spin labeling.[31,38] The two coils were actively decoupled.

Scout anatomic images at three orthogonal axes were acquired to guide placement of a single imaging slice bisecting the center of the eye at the position of the optic nerve head. BF MRI was acquired using the continuous ASL technique[31,38] with four-segment, gradient-echo, echo planar imaging (EPI). The continuous arterial spin labeling used a 2.9 second square radiofrequency pulse to the labeling coil in the presence of 1.0 G/cm gradient. Paired images were acquired in an interleaved fashion, one with arterial spin labeling and the other without spin labeling. For the non-labeled images, the sign of the frequency offset was switched to control for undesirable off-resonance (magnetization transfer) effect.[42] The labeling plane is perpendicular to the flow direction at the neck position. The other MRI parameters were: field of view (FOV) = 11.5 $\times$ 11.5 mm, matrix 128 $\times$ 128 (90 $\times$ 90 μm), slice thickness = 1.5 mm, repetition time (TR) = 3.0 seconds per segment (90° flip angle), and echo time (TE) = 14 ms.

Data Analysis. Image analysis used codes written in a technical computing language (Matlab; MathWorks Inc, Natick, MA) and functional MRI (fMRI) analysis software (STIMULATE; University of Minnesota, Minneapolis, MN). Images were acquired in time series, including anatomic images, and corrected for motion and drift before averaging pixel-by-pixel off-line, as described previously.[26] BF signals (S_{BF}) with intensity in unit of mL/g per min were calculated pixel-by-pixel using $S_{BF} = \lambda/T_1 [(S_N - S_L)/(S_L+(2\alpha - 1)S_N)]$,[31] where S_N and S_L are signal intensities of non-labeled and labeled images, respectively; λ is the water tissue-blood partition coefficient and was taken to be 0.9.[43] A whole-retina T_1 value of 1.7 seconds (Nair G, unpublished data, 2008) was used, consistent with the brain T_1 of 1.6 to 1.8 seconds at 7 T.[44] α, the spin labeling efficiency, was measured previously to be 0.8.[31]

BF percent-change color maps overlaid on BF images were obtained for display purposes, using cross-correlation analysis with >90% confidence level by matching the BF signal time courses to the expected stimulus paradigm. To objectively quantify BF and minimize partial-volume effect, automated profile analysis was performed[26] instead of ROI analysis. The retina was first detected using an edge-detection technique. Radial projections perpendicular to the vitreous boundary were then obtained with (3$\times$) spatial interpolation, which allows automated analysis. Such spatial interpolation was confirmed not to significantly alter peak width and height.[26] BF values for the entire retinal thickness were determined as a function of distance from the optic nerve head. BF profiles were also plotted across the thickness of the retina and averaged along the entire length of the retina. BF value was taken at the peak of the profile as opposed to area under the curve because retinal thickness changed in RCS rats.

Baseline BF was taken before each hypercapnic and hyperoxic challenge (6 minutes of data). The data during the transition to the new gas (2 minutes of data) were discarded. BF for the physiologic stimulation period was obtained after the signal had reached steady state (4 minutes of data). We have previously shown that steady state is reached within 1 to 2 minutes after switching to a new gas (either 5% CO_2 or O_2) where BF and oxygenation (i.e., BOLD fMRI) in the rat brain were imaged under essentially identical setup.[40]

Reported values were in mean $\pm$ SD and error bars were standard errors of the means. All statistical tests used Student's t-test with $P < 0.05$ indicating statistical significance.

RESULTS

Basal BF Measurements

Figure 1A shows a quantitative BF image of a normal retina. To confirm that BF was the source of the signals, measurements were repeated after rats were killed in the scanner. Figure 1B
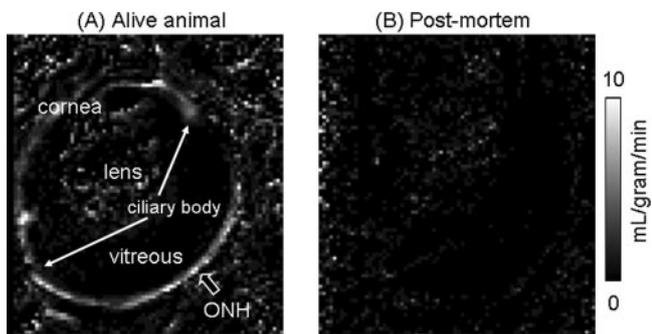
FIGURE 1. Cross-sectional images showing quantitative basal blood flow maps at 90×90 μm from a (**A**) live and (**B**) postmortem rat retina (same animal). *Large arrows* indicate the locations of the optic nerve head (ONH). The scale bar indicates blood flow values in mL/g per min.

FIGURE 3. Group-averaged blood flow as a function of distance from the ONH from a normal Long-Evan rat retina and a RCS rat retina. Data were obtained from one distal edge to another (point a to b).

shows the BF image postmortem. No significant BF contrast was detected postmortem.

Representative BF images of a P90 control rat and a P90 RCS rat are depicted in Figure 2A. There were significant quantitative BF differences between normal and RCS retinas. Figure 2B shows the BF profiles across the retinal thickness of the same pair of control and RCS rat retinas. BF in the P90 normal retina was ~5.5 mL/gram per min, significantly higher than those reported in the brain (~1 mL/gram per min) under essentially identical experimental conditions.[33,45] Basal BF in the RCS rat retinas was markedly diminished compared to the age-matched controls.

The full-width at half maximum (FWHM) of the blood flow profile was 190 μm (group average = 198 ± 20 μm). Previous determination of retinal thickness including the choroid by anatomic MRI reported a value of 267 ± 31 μm.[26] Because retinal BF is expected to be lower than choroid BF, BF FWHM is expected to smaller than anatomic FWHM.

Group-averaged BF as a function of distance from the optic nerve head for control and RCS rat retinas at P90 is depicted in Figure 3. Basal BF in the RCS rat retinas was significantly diminished across the entire retinal length relative to controls.

BF Response to Hyperoxia and Hypercapnia

Representative BF percent-change maps associated with hyperoxic and hypercapnic challenges from a normal animal are depicted in Figure 4. Hyperoxia decreased BF due to vasoconstriction, whereas hypercapnia increased BF due to vasodilation. Active pixels are predominantly localized on the retina.

Figure 5A summarizes the results of the hyperoxia experiments for P90 and P220 RCS rat and their age-matched con-
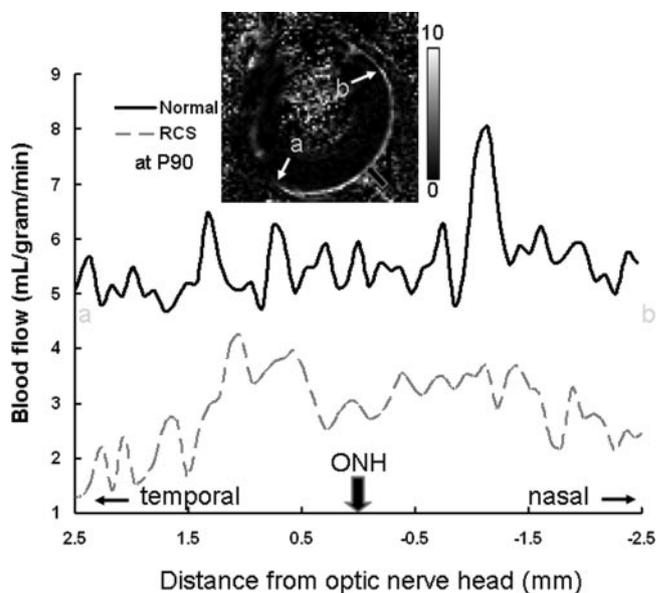
trols. Under basal conditions, normal P90 BF was significantly higher than P220 ($P < 0.05$), suggesting an age-dependent effect. Hyperoxia significantly decreased BF in both normal and RCS rat retinas ($P < 0.05$); absolute hyperoxia-induced BF changes were not statistically different between RCS and normal controls.

Figure 5B summarizes the results of the hypercapnia experiments for P90 and P220 RCS rat and their age-matched controls. Under basal conditions, normal P90 BF was significantly higher than P220 ($P < 0.05$). Hypercapnia significantly increased BF in both normal and RCS rat retinas ($P < 0.05$); absolute hyperoxia-induced BF changes were not statistically different between RCS and normal controls ($P > 0.05$).

Note that basal BF data were obtained immediately before hypercapnic or hyperoxic challenge to minimize the effect of potential physiological fluctuations. In normal animals, basal BF values were not statistically different between the hyperoxia and hypercapnia groups. In RCS animals, basal BF values in the RCS groups were slightly different between the hypercapnia and the hyperoxia group, likely due to comparatively larger biological (i.e., disease related) scattering and lower BF contrast.

Figure 6 shows the corresponding hyperoxic and hypercapnic responses in percentages. Blood-flow percentage changes in RCS retinas were significantly larger than in normal retinas
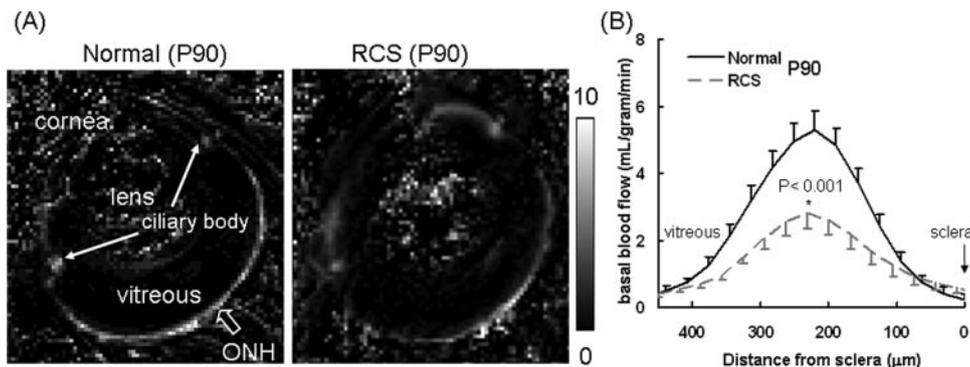
FIGURE 2. (**A**) Blood flow images from a normal retina and a RCS rat retina at postnatal day 90, and (**B**) their blood flow profiles across the retinal thickness. *Large arrows* indicate the locations of the ONH. The scale bar indicates blood flow values in mL/g per min. Error bars are intra-animal variations (SEM) from repeated measurements on one animal. Note that for profile analysis, the original resolution was 90×90 μm and the images were interpolated three times to allow automated analysis.

FIGURE 4. Blood-flow percent-change maps responding to physiologic stimuli of (**A**) 100% O_2 and (**B**) 5% CO_2 obtained from a normal Long-Evan retina. Percent-change color maps are overlaid on blood-flow images with color bars indicating blood-flow percent changes.
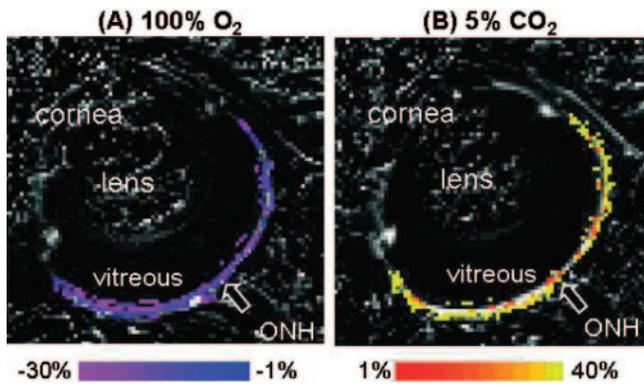
due to lower basal blood flow in RCS retinas (except for the P220 normal controls).

DISCUSSION

This study reports a novel application of MRI to quantitatively image BF and hypercapnia- and hyperoxia-induced BF changes in normal and degenerated retinas. The major findings were that basal BF and stimulus-induced BF changes in the retina can be quantitatively measured, which allows comparison across experimental groups; basal BF in the retina was higher than published basal cerebral BF under essentially identical conditions; BF in the retina was significantly diminished in the degenerated retina; robust hypercapnia- and hyperoxia-induced BF changes were observed in normal retinas; and absolute hypercapnia- and hyperoxia-induced BF changes were similar between normal and RCS retinas, but percent changes were statistically different due to lower basal BF in the RCS rat retinas. These results suggest that vascular reactivity may not be perturbed in retinal degeneration. These results also suggest caution in interpreting differences in relative functional MRI signals in disease states in which basal BF is significantly altered.

Measurement Stability and Partial-Volume Effects

High-resolution MRI of the thin retina is susceptible to drift and movement artifacts. Demands on magnetic field gradient by high-resolution imaging pulse sequences can lead to temperature-induced frequency and signal drift. Perfusion imaging, which requires subtraction of paired images, in particular, may be more sensitive to movement between paired image acqui-
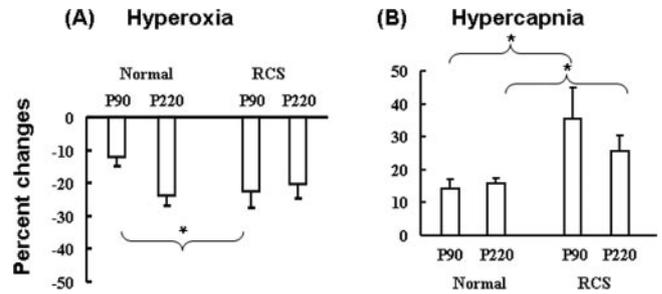

FIGURE 6. Group-averaged blood-flow percent changes of the hyperoxia and hypercapnia experiments for normal and RCS rat retinas. Error bars represent SEM, *$P < 0.05$.

sitions. Hardware stability has previously been evaluated and verified in phantom studies.[26] In addition, the eye may drift slightly over time. We used a combination of isoflurane anesthetic and pancuronium paralytic, which has been demonstrated to essentially eliminate ocular movement over long imaging times.[26] Images were acquired in time series and co-registered as needed before additional data processing (i.e., signal averaging and cross-correlation analysis). Time-loop movies, and signal and center-of-mass time courses were also evaluated to exclude sudden movement or significant drift. These evaluations provided sensitive indicators because signal contamination from either side of the retina due to mis-registration would markedly affect signal intensities.

While the spatial resolution is high compared to typical MRI of rat brains, partial-volume effect may still be significant due to the small transverse dimension and curved geometry of the retina. The 1.5-mm slice thickness was determined to have a partial-volume effect up to 30% of the total retinal thickness due to the retinal curvature (assuming a spherical rat eye of 6-mm diameter).[26] In this study, the in-plane resolution of 90 × 90 μm yielded approximately three pixels across the retinal thickness. This spatial resolution could not selectively resolve BF arising from the retinal or choroidal vascular layer, or reveal the avascular layer between the two vascular layers. Future studies will focus on improving spatial resolution and sensitivity. Nonetheless, the current spatial resolution is sufficient to robustly measure basal BF and BF changes across the entire retinal thickness.

BF and BF Responses in Normal Retinas

Basal BF. BF in the whole retina and the ciliary body were high, whereas BF in the cornea and vitreous were essentially absent or within noise level. Basal BF of the normal retina, is in good agreement with a previous report of 6.3 ± 1.0 mL/gram per min using the same technique.[46] Interestingly, basal BF of
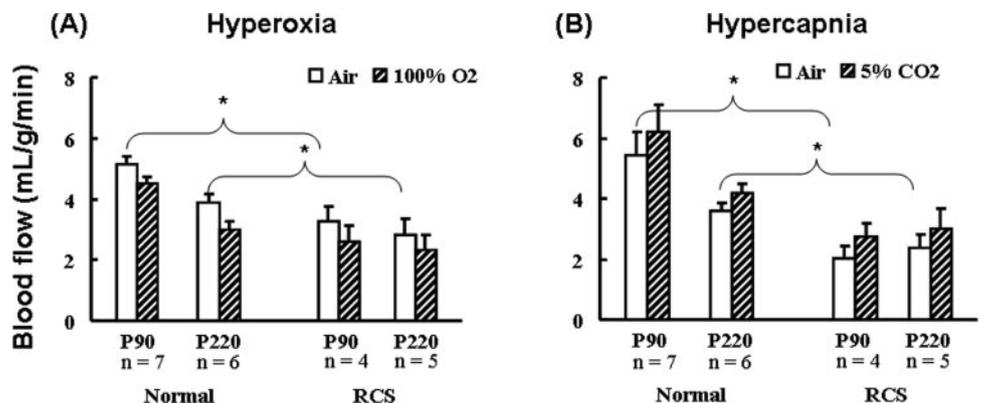

FIGURE 5. Group-averaged quantitative blood-flow data obtained from the (**A**) hyperoxia and (**B**) hypercapnia experiments for normal and RCS rat retinas. Error bars represent SEM.

the whole retina is markedly higher than cerebral BF which has been reported to be 0.9 ± 0.13 mL/gram per min[45] to 1.1 ± 0.04 mL/gram per min[33] under essentially identical experimental conditions, including 1.1% isoflurane anesthesia. BF reported at the current spatial resolution is an average of retinal and choroidal BF. The choroidal BF is about 10 times higher than either cerebral or retinal BF, as determined by the microsphere technique.[47,48] High choroidal BF appears to be in excess of local metabolic requirements. It has been suggested that high choroidal BF may be necessary to maintain a large oxygenation gradient[49] and/or to dissipate heat produced by light,[50,51] although these hypotheses remain to be proven.

BF along the retina is relatively uniform (rats do not possess a fovea). This appears to contradict the notion that the optic nerve head is densely populated by large arteries and veins. However, the ASL technique is generally less sensitive to large vessels and more sensitive to smaller vessels (such as arterioles, capillaries, and venules).[29,34] This is because ASL MRI can be tailored to be more sensitive to BF in smaller vessels by adjusting measurement parameters to minimize large vessel contributions. First, inclusion of a delay (i.e., 200 ms) between arterial spin labeling and image acquisition allows labeled spins to leave large arteries and move into smaller vessels, thereby decreasing sensitivity of large arteries. Second, the labeled spins lose substantial contrast (with a time constant T_1 of ~2 seconds) by the time they reach large draining veins, thereby decreasing the impact of large veins. In short, ASL MRI can be tailored to more selectively detect BF in smaller vessels, although the exact weighting of ASL signals from different vessel sizes is difficult to quantify. Selectively detecting BF in smaller vessels is advantageous, since it more accurately reflects local tissue perfusion. It is also interesting to note that, in contrast to most optically based approaches, MRI measures tissue perfusion of labeled water in the whole tissue within a voxel without the need to resolve individual vessels.

Hyperoxia. Hyperoxia reduced total BF in the retina of normal animals by 12%. Oxygen breathing constricts vessels in the brain and the retina, resulting in BF reduction. Oxygen breathing has been reported to decrease BF in the retina by 30% using LDF,[52] 36% using blue field entoptic technique,[53] and 60% using LDF.[54–56] Similar observations were also reported using oxygen electrodes[7] and laser speckle imaging.[20,21] Most of these optical imaging techniques are sensitive to surface retinal vessels with unknown contributions from the choroid. Interestingly, it has been reported that inhalation of oxygen has little effect on choroidal BF when measured using LDF in the human macula where retinal vessels are absent.[57–59] Given that the choroid BF is about ten times higher than retinal BF, and that choroidal BF appeared to respond weakly to hyperoxia, the overall BF changes detected by MRI are expected to be smaller than compared to optical imaging techniques that are mostly sensitive to the retinal vasculature as was indeed observed. By comparison, oxygen breathing only decreases BF by 13% in awake human brain,[60] suggesting the retinal vessels are substantially more responsive to hyperoxia.

Hypercapnia. Hypercapnia increased total retinal BF by 14% in normal animals. Hypercapnic breathing causes vasodilation in the brain, resulting in BF increase. While there is evidence from LDF and microsphere techniques[61–64] that hypercapnia elicits vasodilation in both retinal and choroidal blood vessels, with the retinal vessels vasodilating more potently, the literature is sparse and inconsistent. Inhalation of 10% CO_2 in air showed no significant vasodilation in the retinal vessels.[65] Inhalation of carbogen (95% O_2 + 5% CO_2) increased choroidal BF by 12.5% ± 11.7%, but inter-subject variations were large.[66] At higher CO_2 concentrations, however, retinal BF was observed to increase 240% and choroidal BF was observed to increase 150% (arterial pCO_2 = 80.9 mm Hg, which

we estimated to be >15% CO_2 effectively).[61] Consistent hypercapnia-induced cerebral BF changes have been reported for awake humans and animals under various anesthetics. Given that choroidal BF is about ten times higher than retinal BF, and that choroidal BF appeared to respond weakly to hypercapnia, the overall BF changes detected by MRI are expected to be smaller than when measured using optical imaging techniques that are mostly sensitive to the retinal vasculature, as was indeed observed. By comparison, hypercapnia increased BF in the brain by 25%[40] and 52%[33] under essentially identical experimental conditions, including 1.1% isoflurane anesthesia.

BF and BF Responses in Retinal Degeneration

Substantial thinning of the retina due to photoreceptor degeneration has been reported by P90 in RCS rats.[5] The total retinal thickness, including the choroid, in P120 RCS rats was 169 ± 13 μm by MRI and 169 ± 23 μm by histology. This compares with 267 ± 31 μm by MRI and 205 ± 11 μm by histology in normal rat retina.[26] Gd-DTPA experiments, although confounded by some partial volume effect, suggested that the debris layer present in the degenerated retina of RCS rats is permeable to Gd-DTPA.[26] Breakdown of the blood-retinal barrier to horseradish peroxidase, invasion of retinal-pigmented-epithelium cells into the outer nuclear layer, and neovascularization in RCS retina have been reported.[67]

With the observed structural changes, it is reasonable to postulate that blood oxygenation, BF, blood volume, and their responses to physiological challenges are perturbed in the P90 RCS rat retinas. Indeed, attenuated BOLD responses to hyperoxia and hypercapnia have been reported in P120 RCS retinas.[26] Diminished layer-specific BOLD response in the choroidal vasculature is perhaps not surprising since the choroid supplies oxygen to the outer nuclear layer. The reduced BOLD response in the retinal vascular layer could be a secondary effect of photoreceptor degeneration that subsequently induces inner retinal degeneration. Abnormal retinal oxygen profiles in RCS retinas under basal conditions have also been reported, using oxygen electrode measurements.[7]

In the present study, basal BF in RCS rat retinas was markedly reduced compared to that of control rat retinas. Given that BF is tightly coupled to basal metabolic activity, reduced basal metabolism of degenerated retinas of P90 RCS rats are expected to lead to reduced basal BF. We found no publication describing LDF and intrinsic optical imaging of the RCS retinas for comparison. There is a substantial literature on brain that supports the notion of diminished BF in many neurodegenerative diseases.[35–37]

Hypercapnia- and hyperoxia-induced absolute BF changes were not statistically different between normal and RCS retinas. Because of the diminished basal BF in the RCS rat retinas, their percent changes were, however, statistically greater than normal. These results suggest that vascular reactivity per se may not be perturbed in retinal degeneration. These findings, if confirmed, could have important implications for fMRI measurement based on percent changes.

In normal animal brains, absolute and relative fMRI signal changes due to forepaw stimulations have been studied under different basal BF and oxygenation by changing inhaled O_2 and CO_2 concentrations. After forepaw stimulation, absolute BF and normalized forepaw stimulation induced BOLD changes were independent of mild perturbations in basal BF and oxygenation. In contrast, forepaw stimulation induced BF and BOLD percent changes varied substantially with mild perturbations of basal BF and oxygenation for the same stimulation parameters. These findings suggest caution in interpreting percent-change fMRI of disease states in which basal BF and oxygenation are perturbed, such as in stroke, aging, and neu-

rodegenerative diseases. In brief, these results underscore the importance of measuring absolute physiologic parameters, as they are likely to be important in interpreting fMRI signal changes in disease states.

Corroborative findings associated with retinal degeneration have been extensively reported using oxygenation electrode techniques. In several studies, Yu and colleagues[7,68,69] examined the RCS rats and found higher dissolved oxygen levels in the remaining outer retina and a significant alteration in the oxygen flux from the choroid to the inner retina, together with the reduced oxygen input from the deeper capillary layer of the retinal circulation. In Abyssinian cats,[70,71] another model of hereditary retinal degeneration, the average inner retinal oxygen tension remained within normal limits at all disease stages, despite the observed progressive retinal vessel attenuation. Loss of photoreceptor metabolism allows choroidal oxygen to reach the inner retina, attenuating the retinal circulation.

Finally, it needs to be stated that while LDF, microsphere, and MRI techniques all measure BF, they use different signal sources, and comparisons need to be made with caution. Microsphere techniques may be susceptible to postmortem artifacts and the reported BF values vary depending on microsphere size and concentration.[48] LDF measures BF at a single point. Retinal BF measurements with LDF are contaminated by signals arising from choroidal BF, and choroid BF measurements are limited to the macula where retinal vessels are absent. In general, most optical imaging techniques used to measure BF are heavily impacted by surface vessels. MRI measures BF over a larger area and is more sensitive to smaller vessels. However, MRI requires longer acquisition times and has lower spatial resolution compared to optical imaging techniques. At the MRI spatial resolution reported here, the measured MRI BF is a weighted average of retinal and choroid BF. BF MRI is not limited by depth resolution and has the potential to image layer-specific BF if higher spatial resolution can be achieved and this is under investigation.

Conclusions

This study demonstrates a novel MRI application to image quantitative BF and hypercapnia- and hyperoxia-induced BF changes in the normal and degenerated retinas. BF MRI has the potential to complement existing retinal imaging techniques. Future studies will focus on improving spatial resolution to distinguish lamina-specific BF in the retinal and choroidal vasculature, investigating visually evoked BF responses, and studying RCS rat retinas at earlier time points to determine the onset of perturbation in layer thicknesses, anatomic MRI contrasts, BOLD fMRI, and basal and hypercapnia- and hyperoxia-induced BF changes. While noninvasive MRI is fully applicable to human studies, clinical translation could be hindered by eye movement and limited spatiotemporal resolution. We are hopeful that these technical challenges can be overcome with rapid advances in MRI technologies (i.e., parallel imaging techniques, sensitive detectors, and magnetic field gradient hardware). Nonetheless, this approach should readily serve as a valuable tool to study BF in animal models of retinal diseases.

References

1. Berson EL. Retinitis pigmentosa. The Friedenwald lecture. *Invest Ophthalmol Vis Sci.* 1993;34:1659–1676.

2. Bourne MC, Campbell DA, Pyke M. Hereditary degeneration of the rat retina. *Brit J Ophthalmol.* 1938;22:613–623.

3. D'Cruz PM, Yasumura D, Weir J, et al. Mutation of the receptor tyrosine kinase gene Mertk in the retinal dystrophic RCS rat. *Hum Mol Genet.* 2000;9:645–651.

4. Ball S, Hanzlicek B, Blum M, Pardue MT. Evaluation of inner retinal structure in the aged RCS rat. *Adv Exp Med Biol.* 2003;533:181–188.

5. LaVail MM. Photoreceptor characteristics in congenic strains of RCS rats. *Invest Ophthalmol Vis Sci.* 1981;20:671–675.

6. LaVail MM, Battelle BA. Influence of eye pigmentation and light deprivation on inherited retinal dystrophy in the rat. *Exp Eye Res.* 1975;21:167–192.

7. Yu D-Y, Cringle SJ, Su E-N, Yu PK. Intraretinal oxygen levels before and after photoreceptor loss in the RCS rat. *Invest Ophthalmol Vis Sci.* 2000;41:3999–4006.

8. Sieving PA, Caruso RC, Tao W, et al. Ciliary neurotrophic factor (CNTF) for human retinal degeneration: phase I trial of CNTF delivered by encapsulated cell intraocular implants. *Proc Natl Acad Sci USA.* 2006;103:3896–3901.

9. Acland GM, Aguirre GD, Ray J, Zhang Q, et al. Gene therapy restores vision in a canine model of childhood blindness. *Nat Genet.* 2001;28:92–95.

10. Rizzo JF 3rd, Wyatt J, Humayun M, et al. Retinal prosthesis: an encouraging first decade with major challenges ahead. *Ophthalmology.* 2001;108:13–14.

11. Fujimoto JG, Brezinski ME, Tearney GJ, et al. Optical biopsy and imaging using optical coherence tomography. *Nat Med.* 1995;1:970–972.

12. Fujimoto JG, Pitris C, Boppart SA, Brezinski ME. Optical coherence tomography: an emerging technology for biomedical imaging and optical biopsy. *Neoplasia.* 2000;2:9–25.

13. Shonat RD, Richmond KN, Johnson PC. Phosphorescence quenching and the microcirculation: An automated, multipoint oxygen tension measuring instrument. *Rev Sci Instrum.* 1995;66:5075–5084.

14. Grinvald A, Bonhoeffer T, Vanzetta I, et al. High-resolution functional optical imaging: from the neocortex to the eye. *Ophthalmol Clin North Am.* 2004;17:53–67.

15. Zarella MD, Li H, Kwon Y, et al. The origins and spatio-temporal properties of stimulus dependent intrinsic optical signals of the retina. In: *Proceedings of the Society for Neuroscience*; Oct. 23–27, 2004; San Diego, CA. Program 934.910.

16. Zhao YB, Yao XC. Intrinsic optical imaging of stimulus-modulated physiological responses in amphibian retina. *Opt Lett.* 2008;33:342–344.

17. Preussner PR, Richard G, Darrelmann O, et al. Quantitative measurement of retinal blood flow in human beings by application of digital image-processing methods to television fluorescein angiograms. *Graefes Arch Clin Exp Ophthalmol.* 1983;221:110–112.

18. Guyer DR, Yannuzzi LA, Slakter JS, et al. The status of indocyanine-green videoangiography. *Cur Opin Ophthalmol.* 1993;4:3–6.

19. Wajer SD, Taomoto M, McLeod DS, et al. Velocity measurements of normal and sickle red blood cells in the rat retinal and choroidal vasculatures. *Microvasc Res.* 2000;60:281–293.

20. Cheng H, Duong TQ. Simplified laser-speckle-imaging analysis method and its application to retinal blood flow imaging. *Opt Lett.* 2007;32:2188–2190.

21. Cheng H, Yan Y, Duong TQ. Temporal statistical analysis of laser speckle image and its application to retinal blood flow imaging. *Optics Express.* 2008;16:10214–10219.

22. Chauhan BC, Yu PK, Cringle SJ, Yu DY. Confocal scanning laser Doppler flowmetry in the rat retina: origin of flow signals and dependence on scan depth. *Arch Ophthalmol.* 2006;124:397–402.

23. Slakter JS, Yannuzzi LA, Guyer DR, et al. Indocyanine-green angiography. *Curr Opin Ophthalmol.* 1995;6:25–32.

24. Lorentz K, Zayas-Santiago A, Tummala S, Kang Derwent JJ. Scanning laser ophthalmoscope-particle tracking method to assess blood velocity during hypoxia and hyperoxia. *Adv Exp Med Biol.* 2008;614:253–261.

25. Shen Q, Cheng H, Chang TF, et al. Magnetic resonance imaging of anatomical and vascular layers of the cat retina. *J Magn Reson Imaging.* 2006;23:465–472.

26. Cheng H, Nair G, Walker TA, et al. Structural and functional MRI reveals multiple retinal layers. *Proc Natl Acad Sci USA.* 2006;103:17525–17530.

27. Duong TQ, Pardue MT, Thule PM, et al. Layer-specific anatomical, physiological and functional MRI of the retina. *NMR Biomed.* 2008;21:978–996.

28. Duong TQ, Ngan S-C, Ugurbil K, Kim S-G. Functional magnetic resonance imaging of the retina. *Invest Ophthalmol Vis Sci.* 2002; 43:1176–1181.

29. Calamante F, Gadian DG, Connelly A. Quantification of perfusion using bolus tracking magnetic resonance imaging in stroke: assumptions, limitations, and potential implications for clinical use. *Stroke.* 2002;33:1146–1151.

30. Detre JA, Leigh JS, Williams DS, Koretsky AP. Perfusion imaging. *Magn Reson Med.* 1992;23:37–45.

31. Shen Q, Ren H, Cheng H, et al. Functional, perfusion and diffusion MRI of acute focal ischemic brain injury. *J Cereb Blood Flow and Metab.* 2005;25:1265–1279.

32. Muir ER, Shen Q, Duong TQ. Cerebral blood flow MRI in mice using the cardiac-spin-labeling technique. *Magn Reson Med.* 2008; 60:744–748.

33. Sicard KM, Duong TQ. Effects of hypoxia, hyperoxia and hypercapnia on baseline and stimulus-evoked BOLD, CBF and CMRO2 in spontaneously breathing animals. *Neuroimage.* 2005;25:850–858.

34. Duong TQ, Kim DS, Ugurbil K, Kim SG. Localized cerebral blood flow response at submillimeter columnar resolution. *Proc Natl Acad Sci USA.* 2001;98:10904–10909.

35. Grafton ST. PET: activation of cerebral blood flow and glucose metabolism. *Adv Neurol.* 2000;83:87–103.

36. Wolf RL, Detre JA. Clinical neuroimaging using arterial spin-labeled perfusion magnetic resonance imaging. *Neurotherapeutics.* 2007; 4:346–359.

37. Silverman DH, Alavi A. PET imaging in the assessment of normal and impaired cognitive function. *Radiol Clin North Am.* 2005;43: 67–77.

38. Duong TQ, Silva AC, Lee SP, Kim SG. Functional MRI of calcium-dependent synaptic activity: cross correlation with CBF and BOLD measurements. *Magn Reson Med.* 2000;43:383–392.

39. Dowling JE, Sidman RL. Inherited retinal dystrophy in the rat. *J Cell Bio.* 1962;14:73–109.

40. Sicard K, Shen Q, Brevard ME, et al. Regional cerebral blood flow and BOLD responses in conscious and anesthetized rats under basal and hypercapnic conditions: implications for functional MRI studies. *J Cereb Blood Flow Metab.* 2003;23:472–481.

41. Duong TQ, Iadecola C, Kim SG. Effect of hyperoxia, hypercapnia, and hypoxia on cerebral interstitial oxygen tension and cerebral blood flow. *Magn Reson Med.* 2001;45:61–70.

42. Shen Q, Meng X, Fisher M, et al. Pixel-by-pixel spatiotemporal progression of focal ischemia derived using quantitative perfusion and diffusion imaging. *J Cereb Blood Flow and Metab.* 2003;23: 1479–1488.

43. Herscovitch P, Raichle ME. What is the correct value for the brain-blood partition coefficient for water? *J Cereb Blood Flow Metab.* 1985;5:65–69.

44. Barbier EL, Liu L, Grillon E, et al. Focal brain ischemia in rat: acute changes in brain tissue T1 reflect acute increase in brain tissue water content. *NMR Biomed.* 2005;18:499–506.

45. Liu ZM, Schmidt KF, Sicard KM, Duong TQ. Imaging oxygen consumption in forepaw somatosensory stimulation in rats under isoflurane anesthesia. *Magn Reson Med.* 2004;52:277–285.

46. Li Y, Cheng H, Duong TQ. Blood flow magnetic resonance imaging of the retina. *Neuroimage.* 2008;39:1744–1751.

47. Alm A, Bill A. Ocular and optic nerve blood flow at normal and increased intraocular pressures in monkeys (Macaca irus): a study with radioactively labelled microspheres including flow determinations in brain and some other tissues. *Exp Eye Res.* 1973;15:15–29.

48. Wang L, Fortune B, Cull G, et al. Microspheres method for ocular blood flow measurement in rats: size and dose optimization. *Exp Eye Res.* 2007;84:108–117.

49. Linsenmeier RA, Padnick-Silver L. Metabolic dependence of photoreceptors on the choroid in the normal and detached retina. *Invest Ophthalmol Vis Sci.* 2000;41:3117–3123.

50. Parver LM. Choroidal blood flow as a heat dissipating mechanism in the macula. *Am J Ophthalmol.* 1980;89:641–646.

51. Parver LM, Auker CR, Carpenter DO, Doyle T. Choroidal blood flow. *Arch Ophthalmol.* 1982;100:1327–1330.

52. Sternn K, Manapace R, Rainer G, et al. Reproducibility and sensitivity of scanning laser Doppler flowmetry using graded changes in PO2. *Br J Ophthalmol.* 1997;81:360–364.

53. Fallon TJ, Maxwell DL, Kohner EM. Retinal vascular autoregulation in conditions of hyperoxia and hypoxia using the blue field entopic phenomenon. *Ophthalmology.* 1985;92:701–705.

54. Riva CE, Grunwald JE, Petrig BL. Autoregulation of human retinal blood flow. An investigation with laser Doppler velocimetry. *Invest Ophthalmol Vis Sci.* 1986;27:1706–1712.

55. Riva CE, Grunwald JE, Sinclair SH. Laser Doppler velocimetry study of the effect of pure oxygen breathing on retinal blood flow. *Invest Ophthalmol Vis Sci.* 1983;24:47–51.

56. Trokel S. Effect of respiratory gases upon choroidal hemodynamics. *Arch Ophthalmol.* 1965;73:838–842.

57. Riva CE, Cranstoun SD, Grunwald JE, Petrig BL. Choroidal blood flow in the foveal region of the human ocular fundus. *Invest Ophthalmol Vis Sci.* 1994;35:4273–4281.

58. Schmetterer L, Wolzt M, Lexer F. The effect of hyperoxia and hypercapnia on fundus pulsations in the macular and optic disc region in healthy young me. *Exp Eye Res.* 1995;61:685–690.

59. Schmetterer L, Lexer F, Findl O, et al. The effect of inhalation of different mixtures of O2 and CO2 on ocular fundus pulsation. *Exp Eye Res.* 1996;63:351–355.

60. Kety SS, Schmidt CF. The effects of altered arterial tensions of carbon dioxide and oxygen on cerebral blood flow and cerebral oxygen consumption of normal young men. *J Clin Invest.* 1948; 27:484–491.

61. Alm A, Bill A. The oxygen supply to the retina, II: effects of high intraocular pressure and of increased arterial carbon dioxide tension on uveal and retinal blood flow in cats. *Acta Physiologica Scand.* 1972;84:306–319.

62. Alm A, Bill A. The oxygen supply to the retina, I: effects of changes in intraocular and arterial blood pressures, and in arterial pO2 and pCO2 on the oxygen tension in the vitreous body of the cat. *Acta Physiol Scand.* 1972;84:261–274.

63. Friedman E, Chandra SR. Choroidal blood flow, III: effects of oxygen and carbon dioxide. *Arch Ophthalmol.* 1972;87:70–71.

64. Cioffi GA, Granstam E, Alm A. Ocular circulation, In: Kaufman PL, Alm A, eds. *Adler's Physiology of the Eye: Clinical Application.* St. Louis: Mosby 2003;747–784.

65. Frayser R, Hickam JB. Retinal vascular response to breathing increased carbon dioxide and oxygen concentrations. *Invest Ophthalmol Vis Sci.* 1964;3:427–431.

66. Geiser MH, Riva CE, Dorner GT, et al. Response of choroidal blood flow in the foveal region to peroxia and hyperoxia-hypercapnia. *Current Eye Res.* 2000;21:669–676.

67. Wang S, Villegas-Perez MP, Holmes T, et al. Evolving neurovascular relationships in the RCS rat with age. *Current Eye Res.* 2003;27: 183–196.

68. Yu PK, Yu D-Y, Cringle SJ, Su E-N. Endothelial F-actin cytoskeleton in the retinal vasculature of normal and diabetic rats. *Curr Eye Res.* 2005;30:279–290.

69. Yu DY, Cringle S, Valter K, et al. Photoreceptor death, trophic factor expression, retinal oxygen status, and photoreceptor function in the P23H rat. *Invest Ophthalmol Vis Sci.* 2004;45:2013–2019.

70. Kang Derwent JJ, Padnick-Silver L, McRipley M, et al. The electroretinogram components in Abyssinian cats with hereditary retinal degeneration. *Invest Ophthalmol Vis Sci.* 2006;47:3673–3682.

71. Padnick-Silver L, Kang Derwent JJ, Giuliano E, et al. Retinal oxygenation and oxygen metabolism in Abyssinian cats with a hereditary retinal degeneration. *Invest Ophthalmol Vis Sci.* 2006;47: 3683–3689.